ADVANCED OPTICAL MATERIALS
www.advopticalmat.de

Multiplex SERS Phenotyping of Single Cancer Cells in Microdroplets

Kevin Oliveira, Alexandra Teixeira, José M. Fernandes, Cláudia Lopes, Alexandre Chícharo, Paulina Piairo, Lei Wu, Laura Rodríguez-Lorenzo, Lorena Diéguez, and Sara Abalde-Cela**

In the context of personalized medicine, the analysis of single cells is key in order to understand the origin and evolution of cancer to provide an accurate prognosis. Microfluidics and microdroplets are increasingly used for the handling and understanding of the behavior of single cells, as they offer the perfect isolated environment. However, due to the small volumes handled, it is necessary to couple this technology with an ultrasensitive detection technique. Herein, surface-enhanced Raman scattering (SERS) spectroscopy and droplet microfluidics are combined toward the multiplex phenotypic analysis of single cancer cells. For this, cancer cells are labeled with different SERS tags that recognize membrane proteins and encapsulated individually in microdroplets. Afterward, single cells within microdroplets are imaged by SERS spectroscopy. To the best of the authors' knowledge, this is the first time that a multiplex phenotypic SERS analysis of single cells in microdroplets is shown. This integrated optofluidic platform paves the way toward the multiplex and automated characterization of cell populations in cancer patients.

1. Introduction

The reason behind the high mortality of cancer (9.6 million deaths in 2018) is that it is a heterogeneous and dynamic disease and that an average of 60% of patients diagnosed with a primary tumor will relapse, having other tumors spread in their body.[1,2] Consequently, 90% of cancer-related deaths are due to metastasis in secondary organs different from that of the primary tumor.[3] Due to the complicated nature of cancer, a panoply of different inherent factors has been defined as the hallmarks of metastasis: motility and invasion, ability to modulate the secondary site or local microenvironments, plasticity, and ability to colonize secondary tissues.[3] The metastatic cascade has been very well described,[4] and the circulating tumor cells (CTCs) that can originate in the primary tumor appear as one of the main vehicles for the spread of the tumor. The study of single cells is revolutionizing the way we approach and understand cancer supported by the use of new technology developed for biology.[5] Nowadays, by using single-cell omics (genomics, transcriptomics, and/or metabolomics) it is possible to obtain information at the single-cell level and not only averaged data across a bulk population of cells, as in the past.[6] However, the handling of single cells is not a straightforward task to perform in the laboratory, not to mention their downstream analysis. Limitations in terms of reproducibility, high throughput, and automation are hindering the study of single cells.

The increasing need for miniaturization and the continuous developments in microfluidics lead to the implementation of those systems in several fields and branches of science[7] such as biology, chemistry, engineering, biomedical technologies, medical diagnostics, etc.[8–12] Devices used in microfluidics have several advantages on their own as they are simple and cheap to fabricate, as well as capable of reducing the volumes and time needed for a reaction from milliliters to microliters and hours to only several seconds, respectively.[13] This technology branches out to different fashions such as continuous flow,

K. Oliveira, A. Teixeira, C. Lopes, A. Chícharo, P. Piairo, L. Wu, L. Rodríguez-Lorenzo, L. Diéguez, S. Abalde-Cela
International Iberian Nanotechnology Laboratory—INL
Avenida Mestre José Veiga s/n, Braga 4715-330, Portugal
E-mail: lorena.dieguez@inl.int; sara.abalde@inl.int

The ORCID identification number(s) for the author(s) of this article can be found under https://doi.org/10.1002/adom.202201500.

DOI: 10.1002/adom.202201500

A. Teixeira
Life and Health Sciences Research Institute (ICVS)
Escola de Medicina
Universidade do Minho
Campus Gualtar
Braga 4710-057, Portugal

A. Teixeira
ICVS/3B's – PT Government Associate Laboratory
Braga/Guimarães 4710-057, Portugal

J. M. Fernandes
Universidade Nova de Lisboa
Campus da Caparica
Caparica 2829-516, Portugal

droplet-based, paper-based, and digital microfluidics, among others.[14–17] More specifically, droplet-based systems are based on generating monodisperse droplets at very high throughput by using immiscible phases that promote the compartmentalization and parallelization of the single cells. The most common geometry to generate microdroplets is the so-called flow-focusing, which has an intersection between at least three channels, commonly called T-junction. The dispersed phase (solution to be encapsulated) is injected through the central channel, and the continuous phase (immiscible phase) flows to pinch the stream of the dispersed phase through the lateral focusing channels. Finally, the third channel is used as an outlet channel for the droplets that contain the encapsulated elements.[7,13,18–20] The use of microdroplets to encapsulate single-cells spans to different applications such as isolation, sorting, growth, genomic, transcriptomic, and metabolomics studies, among others.[21–26]

Microfluidic devices have been coupled to analytical detection techniques such as Raman spectroscopy, fluorescence microscopy, bright-field microscopy, electrochemistry, capillary electrophoresis, mass spectrometry, nuclear magnetic resonance spectroscopy, absorbance detection, or chemiluminescence.[27] Particular attention should be paid to the impact on the development of new optofluidic devices as a result of the combination of microfluidics and surface-enhanced Raman scattering spectroscopy (SERS).[7,28] SERS is a surface phenomenon that enables the enhancement of the Raman signal of molecules adsorbed (or in close proximity) on a plasmonic metal nanostructure, after excitation with an appropriate wavelength.[29] SERS is considered a powerful fingerprinting and ultrasensitive detection technique that allows for the rapid identification of chemical and biological analytes.[30,31] Techniques used for the analysis of single cells span from fluorescence or mass spectrometry to molecular methods such as PCR or NGS. The chosen technique not only depends on the subject of study (metabolites, proteins, or nucleic acids) but also on the access to those bioanalytes.[32] When compared to those mainstream and more traditional techniques, SERS offers a much higher multiplexing ability using the same excitation source (unlike fluorescence) and avoids photobleaching while ensuring a very high sensitivity.[33] Thus, the use of microdroplets for cancer cell encapsulation in combination with SERS detection can potentially provide a miniaturized and integrated sensing platform with the potential to isolate, identify, and characterize single cells.[21,34]

Herein, we developed a protocol for fast phenotyping of different cancer cell types, based on SERS and microdroplets. In this optofluidic-based platform, we combined three different technologies, where nanoparticles (NPs) were used as a sensing agent to identify the phenotypic characteristics of the cells, microdroplets as a sensing platform to hold the cells, and the sensing technique was SERS spectroscopy. In both cell types, SK-BR-3 and MDA-MB-435 were possible to detect the signal of the Raman reporter in the SERS tag 1-naphthalenethiol (1-NAT) and consequently the expression of epithelial cell adhesion molecule (EpCAM), even in lower levels of expression. Moreover, we confirmed that is possible to use multiplexing assays to perform a fast and very sensitive phenotypic characterization.

2. Results

2.1. Synthesis and Characterization of SERS Tags

In this study, the phenotypic characterization of single cancer cells was based on the use of SERS tags.[35,36] The different steps needed to fabricate the SERS tags are described in **Figure 1**. Gold nanostars (GNSs) were synthesized following a seed-mediate method (Figure 1a-i,ii),[37] and codified with a well-known Raman reporter (RaR), 1-NAT, as indicated in Figure 1a-iii. Mercaptoundecanoic acid (MUA) was used during the codification to ensure the colloidal stability of the GNSs.[38,39] Then, the GNSs codified with 1-NAT (GNSs@1-NAT) were coated with a silica layer (GNSs@1-NAT@SiO_2) to avoid the leakage or destabilization of the RaR, as well as to promote the mechanical stability of the metallic nanoparticles avoiding aggregation (Figure 1b-iv). The silica coating also enabled the functionalization with different chemical groups for the conjugation of the GNSs@1-NAT@SiO_2 with different antibodies recognizing cell membrane proteins,[40] as it is depicted in Figure 1b-v.

Morphological, optical, and spectroscopic characterization were performed to verify the quality of the SERS tags at different control points during the synthetic process. **Figure 2** shows the transmission electron microscopy (TEM) micrographs of the synthesized GNSs before (Figure 2a) and after the silica coating (Figure 2b), demonstrating that the star-shaped NPs are monodisperse and have a homogeneous silica coating. The TEM images were also used to obtain the size distribution of the GNSs (Figure 2c), being 109.4 ± 11.3 nm before silica coating and 134.2 ± 15.6 nm after silica coating (Figure S1, Supporting Information). The comparison of the absorbance spectra of both the non-coated and silica-coated GNSs is shown in Figure 2d. The plasmonic response indicates the size of the core (λ_{max} = 563 nm) and the length and monodispersity of the tips of the GNSs (λ_{max} = 867 nm).[37,41] In this case, it indicates that the nanostars have a size of around 90–110 nm and sharp tips with high monodispersity, which was also confirmed by the TEM analysis. After the silica coating, a small decrease in the intensity and a red-shift of the plasmon band of the tips (located at λ_{max} = 913 nm) for the GNSs@1-NAT@SiO_2 was observed. Furthermore, the characterization of the colloidal stability by dynamic light scattering (DLS) in isopropanol (IPA) (solvent used during the particle preparation) and phosphate-buffered saline (PBS) (medium used in the cell experiments) showed that the GNSs@RaR@SiO_2 remain colloidally stable in PBS (Figure S2 and Table S1, Supporting Information). After verifying that the silica coating was successful, the SERS spectrum of the resulting GNS@1-NAT@SiO_2 was measured. The SERS signal obtained was in agreement with that previously reported for 1-NAT.[42] For this study, two characteristic Raman ring stretching modes at 1377 and 1556 cm^{-1} were used for the subsequent study of the potential of these SERS tags to be used for the characterization of cell membrane surface biomarkers (Figure 2e).

2.2. Single-Cell Encapsulation and Performance of SERS Tags

To evaluate the performance of the synthesized SERS tags, the GNSs@1-NAT@SiO_2 was bioconjugated with an EpCAM

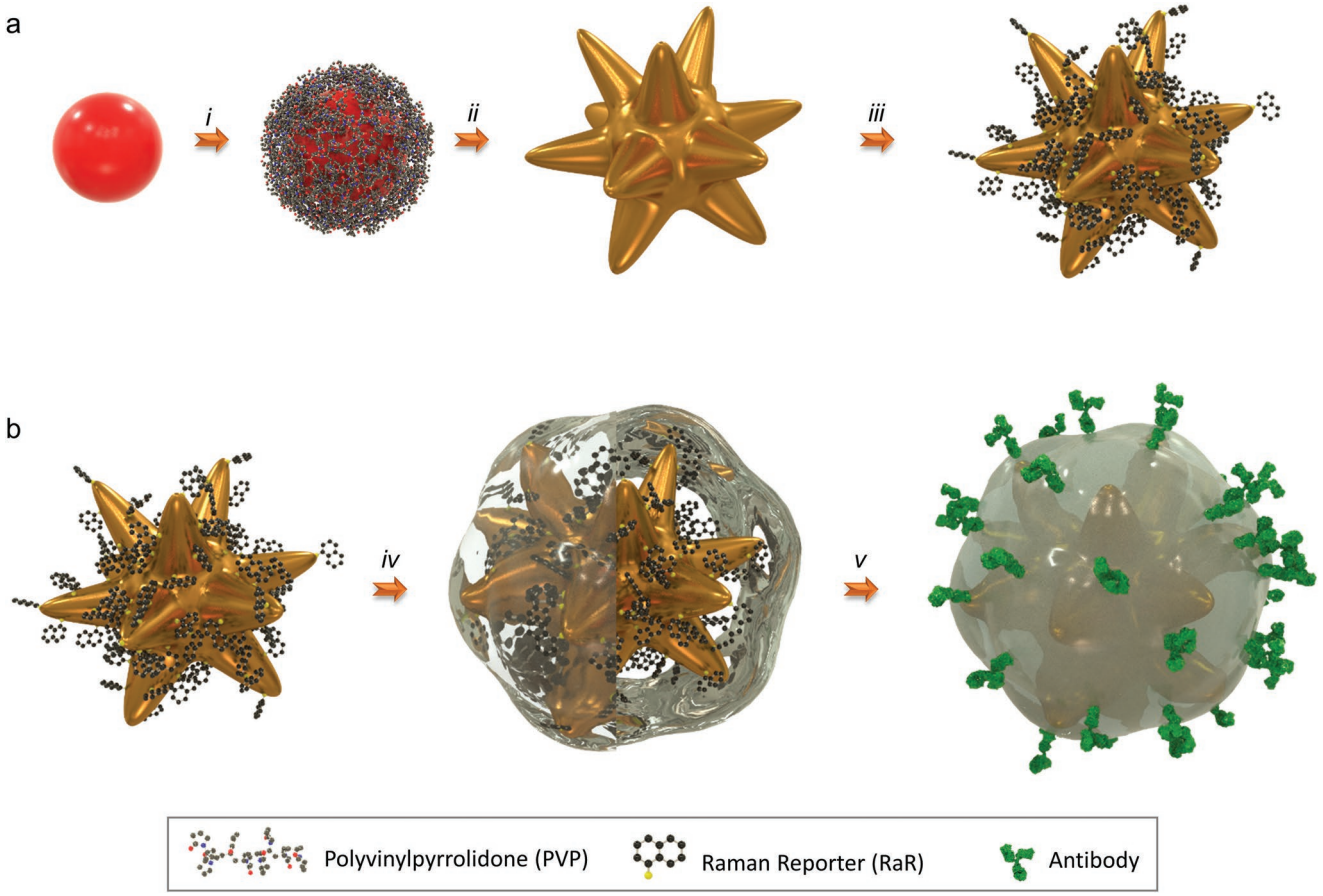

Figure 1. Schematic representation of the synthesis of SERS tags. a) Seed-mediated synthesis of GNSs; i) AuNP seeds of 15 nm that are coated with polyvinylpyrrolidone (PVP) in step (ii) to promote the kinetic control for the growth of anisotropic AuNPs, in this case, GNSs; iii) The GNSs were labeled with 1-NAT to use as RaR for the indirect detection of membrane surface proteins of cancer cells. b) Silica coating and bioconjugation; iv) GNSs@1-NAT were coated with a thin layer of silica to allow the v) biofunctionalization with antibodies that will recognize cancer cells. The elements in this figure are not to scale.

antibody (Figure 1b-v). The EpCAM protein is often used as a CTC biomarker in different types of cancers originating from solid tumors. Specifically, it is expressed on various breast cancer cell lines,[20] and overexpression of this molecule is commonly associated with a poor prognosis of this type of cancer.[43] For a first performance test, the SK-BR-3 cancer cell line, known to have a high expression of EpCAM, was used.[44] After mixing the suspension of SERS tags with the cancer cells for the SERS labeling, the mixture was encapsulated in microdroplets. A scheme depicting the labeling and encapsulation strategy is shown in **Figure 3**.

In order to obtain single cells in each droplet, a specific design of the channels of the microfluidic device was used, based on the Dean Flow Dynamics.[45] The spiral microchannel following the center inlet is used to shift the position of the cells from the convex wall of the channel toward the concave wall (Figure S3, Supporting Information). The resultant microdroplets were then stored in a reservoir composed of an array of 25 µm pillars with an 80 µm gap (Figure S4, Supporting Information) and then measured in situ with a confocal Raman spectrometer.

The SERS spectra resulting from cells labeled with SERS tags conjugated with EpCAM (**Figure 4**a,b) showed positive results. Five cells containing microdroplets were selected in the reservoir for their initial analysis. For each of those microdroplets, the bright-field images (Figure 4a) show almost in most cases single-cell encapsulation. However, microdroplet (v) showed double encapsulation. This may be explained either through the adhesive properties of this cell line or that the cell was dividing at the time of encapsulation. Figure 4b shows the SERS spectrum from each of the five cells analyzed. The characteristic peaks of 1-NAT (1377 and 1556 cm^{-1}) displayed a good intensity demonstrating the binding of the EpCAM antibody to the cell surface. To test the non-specific binding of the SERS tags to the cell surface, a control experiment was performed (Figure 4c,d), in which cells were mixed with unconjugated GNSs@1-NAT@SiO_2. Single spectra measurements were acquired on five static cells encapsulated in microdroplets (Figure 4d). The low or no presence of the 1-NAT signal suggested that the SERS tags before antibody conjugation present low affinity for the cell surface. Single spectrum measurements were also performed on empty droplets (Figure S5, Supporting Information) and as expected, no signal was observed.

Furthermore, to confirm the results obtained in Figure 4, a SERS mapping of a cell encapsulated in a microdroplet was

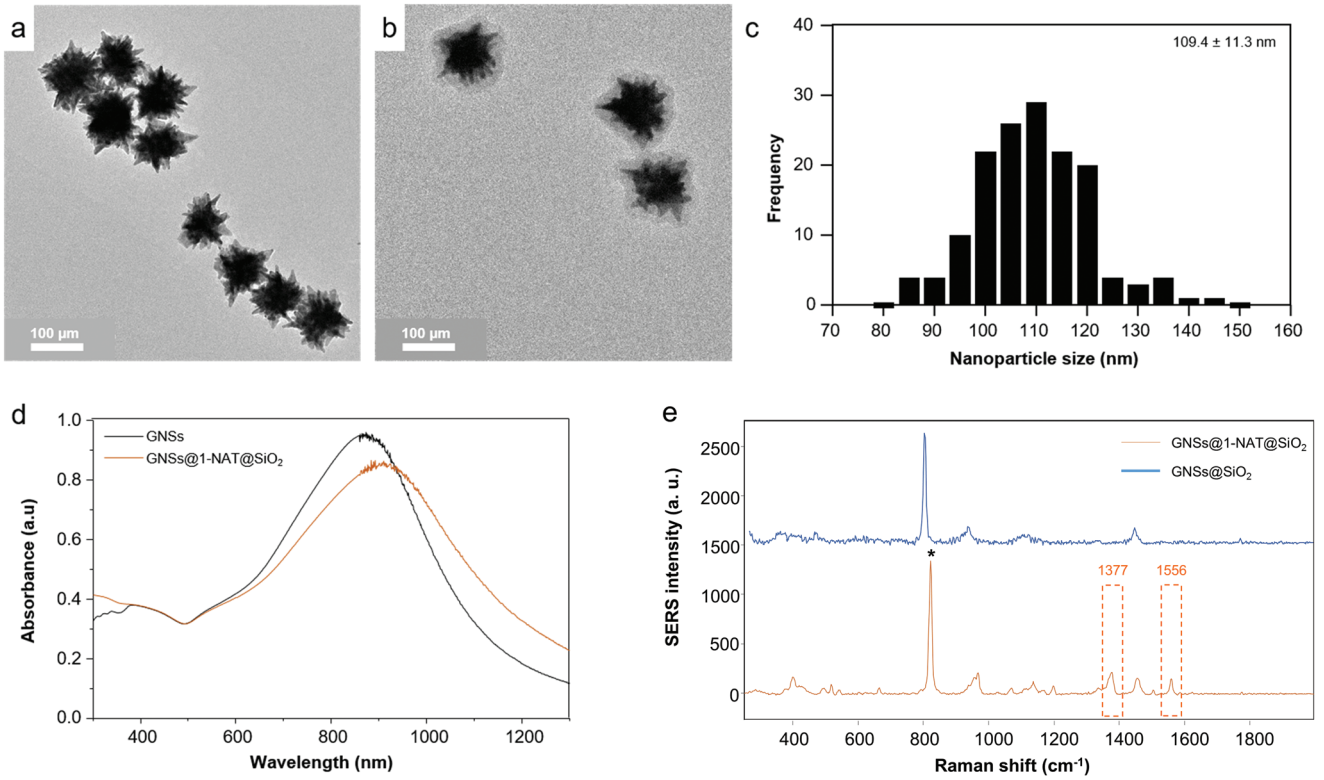

Figure 2. Morphological, optical, and SERS characterization of the SERS tags. a) TEM image of GNSs; b) TEM image of the GNSs after codification with 1-NAT and after the silica coating (GNSs@1-NAT@SiO_2). c) Histogram representing the size distribution of the obtained GNSs. For this, 150 GNSs were measured using Image J and the average size of GNSs was 109.4 nm, with a standard deviation of 11.3 (109.4 ± 11.3). d) Comparison of UV–vis spectra of GNSs and GNSs@1-NAT@SiO_2, normalized at 400 nm. The plasmon band located at 867 nm is related to the tips of the GNSs. The peak located at a maximum wavelength of 563 nm appears as a result of the core of the GNSs. e) SERS spectra resulting from average measurement (liquid SERS measurements) of the GNSs@1NAT@SiO_2 at 1 mM concentration of Au and of the GNS@SiO_2. The characteristic peaks of 1-NAT are highlighted by dashed orange boxes at 1377 and 1556 cm^{-1}. The peak at 821 (cm^{-1}) marked with an asterisk (*) represents the peak of the isopropyl alcohol (IPA), the solvent used for the dispersion of the SERS tags. The shown SERS spectrum is the result of the average of five acquired measurements.

also performed. **Figure 5** shows that the selected characteristic peaks of 1-NAT for GNSs (1377 and 1556 cm^{-1}) had a high intensity across the cell, which varied depending on the area of the map. After these preliminary experiments, it was possible to confirm that the designed SERS tags presented the required performance results to explore their ability for multiplex phenotyping of single cells in microdroplets. Additionally, Figure S6, Supporting Information, shows SERS maps of three additional different cells within a microdroplet and the EpCAM expression monitored through the developed SERS tags.

2.3. SERS-Based Single-Cell Multiplex Phenotyping

According to the previous results (Figure 2e), the GNSs codified with 1-NAT have two specific ring stretching vibrations,[42] at 1377 and 1556 cm^{-1}, which were selected as the peak to identify binding events between SERS tags and cells. For the multiplexing phenotype analysis, two additional RaRs were added, toluidine blue (TB) and nile blue (NB). These molecules are well-known Raman active molecules, and in this way, three different SERS tags or codes were available for testing. The SERS efficiency of the three solutions of GNSs@RaR (1-NAT, TB, and NB) was characterized off-chip (Figure S7, Supporting Information). The Raman fingerprints of each RaR (in liquid) were compared to the background Raman spectra of the different materials (polydimethylsiloxane; PDMS) and solutions (oil and surfactant) that were used during the on-chip analyses (Figure S7, Supporting Information). This was done to avoid the overlapping of the selected peaks for each RaR with the signal given by the background elements. Characteristic peaks of these two additional RaRs, not overlapping with background spectra, were identified at 1613 cm^{-1} (ring stretching vibration)[46] for TB and at 585 cm^{-1} for NB (ring in-plane deformation).[47] To demonstrate not only the multiplex capability of this approach but also its application on different cancer cell lines, this experiment was performed using the MDA-MB-435 cell line. This cell line was traditionally considered a breast cancer line, however, it has been recently re-classified as a melanoma cell model.[48] The EpCAM expression of MDA-MB-435 is not as high as for SK-BR-3,[44,49,50] being a more challenging model to test the performance of these SERS tags. The selection of the panel of antibodies was composed of EpCAM, Vimentin, and CD45. EpCAM is a type I transmembrane glycoprotein[51] and Vimentin is a cytoskeletal protein, which is expressed in breast and melanoma cancer cells with a mesenchymal phenotype.[52,53] Vimentin was included to study the specificity of the assay and discriminate non-specific attachment, as this

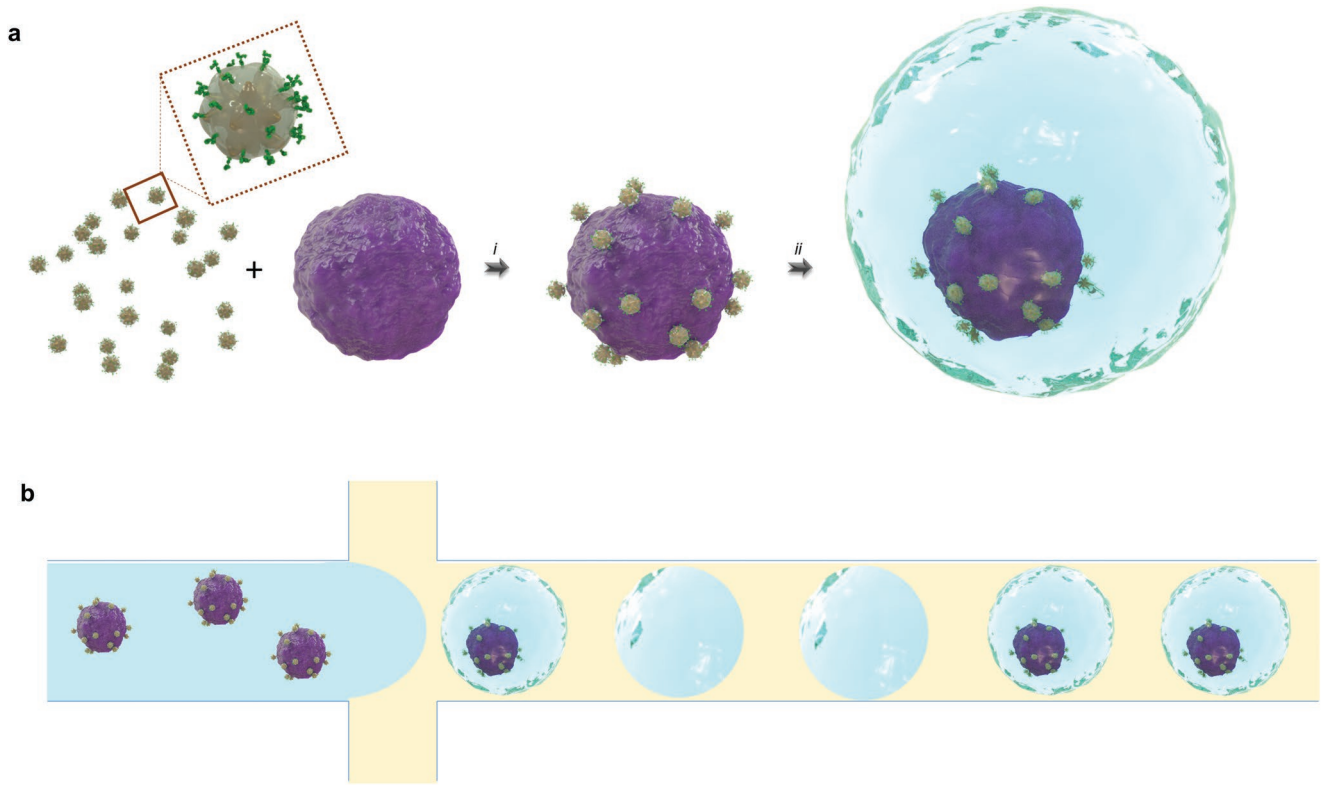

Figure 3. a) Schematic representation of the labeling of cancer cells (purple spheres) with i) SERS tags and their encapsulation in microdroplets for ii) single-cell analysis and b) scheme depicting the encapsulation process, in which the cells labeled with the SERS tag come along a central microfluidic channel (blue) and the contents of that channel are pinched off by two transversal streams of the fluorinated oil and surfactant (yellow) to create droplets. The elements in this figure are not to scale.

protein is expressed intracellularly, and thus, no SERS signal was expected for the samples with the SERS tags paired to Vimentin. CD45, used as a negative control, is a transmembrane protein present in hematopoietic cells.[54] The expression of EpCAM and Vimentin in the cell line used in this set of experiments was confirmed by an immunofluorescence assay (Figure S8, Supporting Information). In order to verify the presence of surface proteins in the MDA-MB-435 cells line, each corresponding antibody was paired to a different SERS tag: EpCAM was coupled to 1-NAT, Vimentin to TB, and CD45 to NB. **Figure 6** shows the SERS spectrum after analyzing five different cells. Taking into account the selected bands for each of the biomarkers (Figure S6, Supporting Information), the characteristic vibrational bands of 1-NAT were present with a slight shift (from 1377 to 1372 cm^{-1}), but with high intensity in all acquired spectra from the five different cells. The latter indicates that those cells express EpCAM and that it can be detected at the single-cell level using SERS tags in a microdroplet environment. In contrast, the characteristic vibrations of TB and NB (1613 and 585 cm^{-1}) were almost non-existent when compared to those of the 1-NAT, matching expected results for these negative controls. Since expression varies along the membrane, a SERS map of a single cell was acquired (area of 20 µm × 20 µm, 1 µm step size) (**Figure 7**). These results demonstrate the variation of the intensity of the characteristic vibrations of the 1-NAT across the same cell, which may be related to the variability of the EpCAM expression on different areas of the cell membrane.

As shown in Figure 7, by mapping the chosen characteristic peaks for each RaR, we were able to confirm the previously obtained results shown in Figure 6. The characteristic peak of 1-NAT could be detected across the cell, which may vary depending on the spot where the laser is pointed and the EpCAM expression. However, the bands of TB and NB were almost non-existent and can be considered as either noise or also due, in the case of the TB, to slight effects related to non-specific absorption.

3. Discussion

Herein, we have developed a novel technology for the phenotypical characterization of single cancer cells using the combination of microdroplets and SERS. The SERS strategy and substrate chosen for this work were based on the use of anisotropic gold NPs. Aspects such as size, shape, composition, and stability should be cautiously controlled because they are crucial to achieve sensitive and reproducible SERS detection. More specifically, gold was chosen as it offers better control and reproducibility over the particle size and shape, being more chemically inert and robust than silver.[55] Despite silver, a priori, showing a higher SERS enhancement, the fact of having anisotropic NPs (GNSs) accounts for the difference in the enhancement of silver versus gold.[56] Regarding the strategy, one of the main advantages of using SERS tags for the characterization

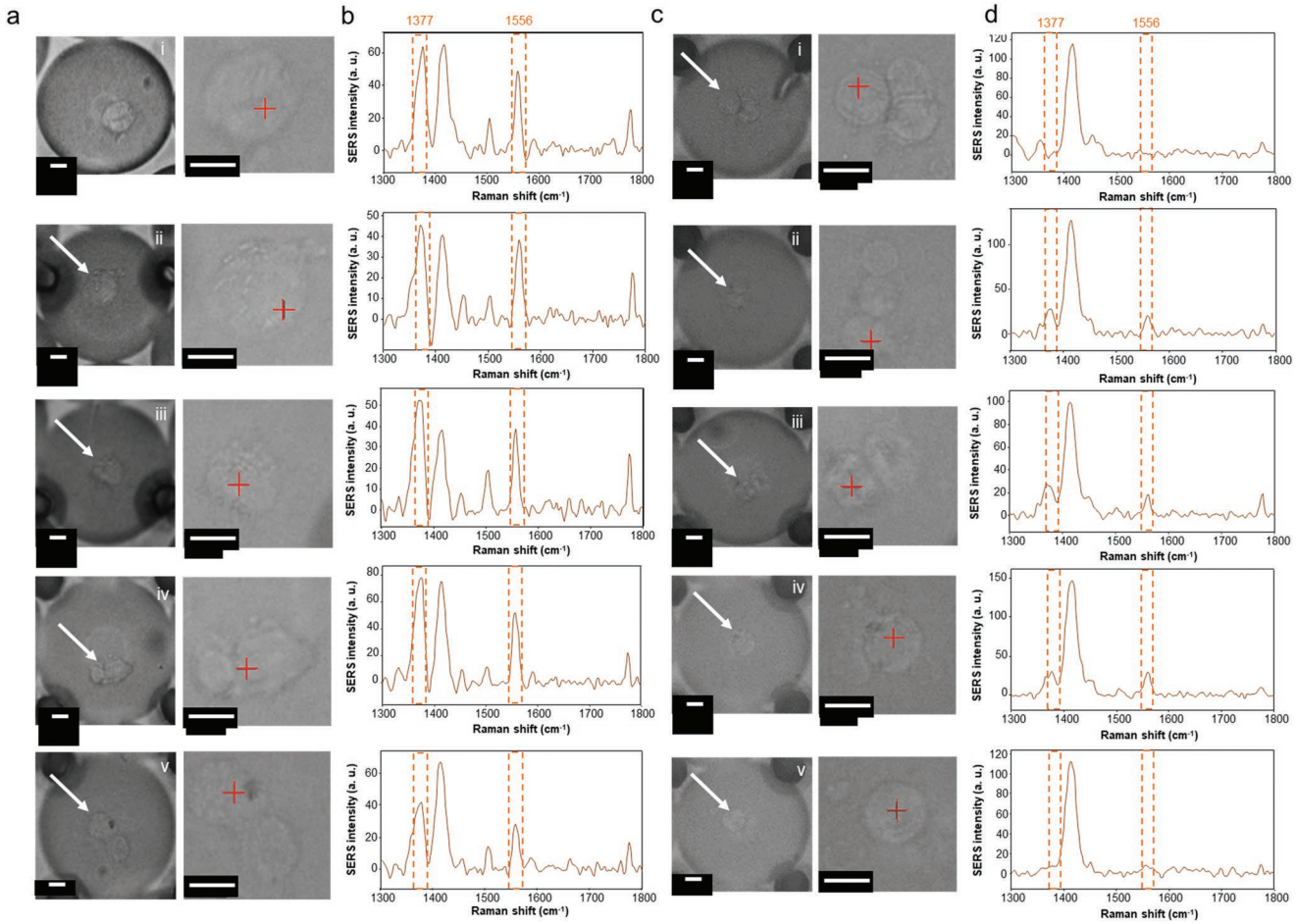

Figure 4. Evaluation of the a,b) performance and c,d) specificity of the SERS tags for the phenotypic characterization of the SK-BR-3 cell line. a) Five bright-field images of five different cells containing microdroplets at low (left) and high magnification (right). b) SERS spectra acquired at the surface of each of the five single-cells displayed in (a) after labeling with GNSs@1-NAT@SiO_2@EpCAM. The SERS characteristic peaks of 1-NAT (1377 and 1556 cm^{-1}) are highlighted in the dashed boxes, which report the presence of the EpCAM protein on the surface of the cell. c) Five bright-field images of five different cells containing microdroplets at low (left) and high magnification (right) used for the evaluation of non-specific interactions of NPs with SK-BR-3 cells. d) SERS spectra acquired at the surface of each of the five single cells displayed in (c) after labeling with GNSs@1-NAT@SiO_2. In this case, the intensity of the SERS characteristic peaks of 1-NAT (1377 and 1556 cm^{-1}) is much lower than that shown in (b), indicating that the non-specific interactions of the SERS tags without an antibody are not significant. All Raman spectra are composed of an average of five acquired measurements. Scale bar 20 μm.

is the high multiplexing capability that can be achieved when compared to label-free SERS.[57] For instance, the use of SERS tags (also known as SERS codified, encoded, or barcoded NPs) has demonstrated to be of use in bio and nanomedicine. Some examples that can be found in previous literature applied the SERS tags strategy in multiplex DNA analysis,[58] serological marker classification,[59] protein expression in vitro[60] and in vivo assays,[61] or even for multiplex cell discrimination.[62] In particular, the use of GNSs for the synthesis of SERS tags is a widely adopted strategy as they offer an extra enhancement of the SERS signal.[63–65] Traditionally, the most established technique for the analysis of different biomarkers is fluorescence in all its diverse fashions, from immunofluorescence to flow-cytometry or fluorescence-activated cell sorting (FACS). However, fluorescence techniques are limited by the number of fluorochromes that can be identified simultaneously (4 to 6).[66] In comparison, SERS has the potential of identifying a much larger number of biomarkers due to the narrow peaks of Raman reporters in comparison with fluorescence, with the added advantage of using the same excitation source. Thus, as long as the characteristic vibrations of those reporters do not overlap, they can be easily identified in the same SERS combined spectra. In this work, we have demonstrated a further and novel use of SERS and microdroplets, presenting for the first time the phenotypic SERS characterization in microdroplets. Figure 5 shows a map of the SERS phenotyping of a single cell encapsulated in microdroplets using one specific type of SERS tag. To the best of our knowledge, this is the first report of the SERS imaging of an isolated single cell. On the one hand, previous works benefiting from microdroplets technology for the imaging of single cells have been mostly focused on the use of fluorescence imaging, limiting the number of biomarkers that can be studied at the same time.[67,68] On the other hand, SERS imaging of cells based on protein expression has been reported. For example, Nima et al. demonstrated the analysis of the phenotype of CTCs using this strategy, but in a bulk experiment

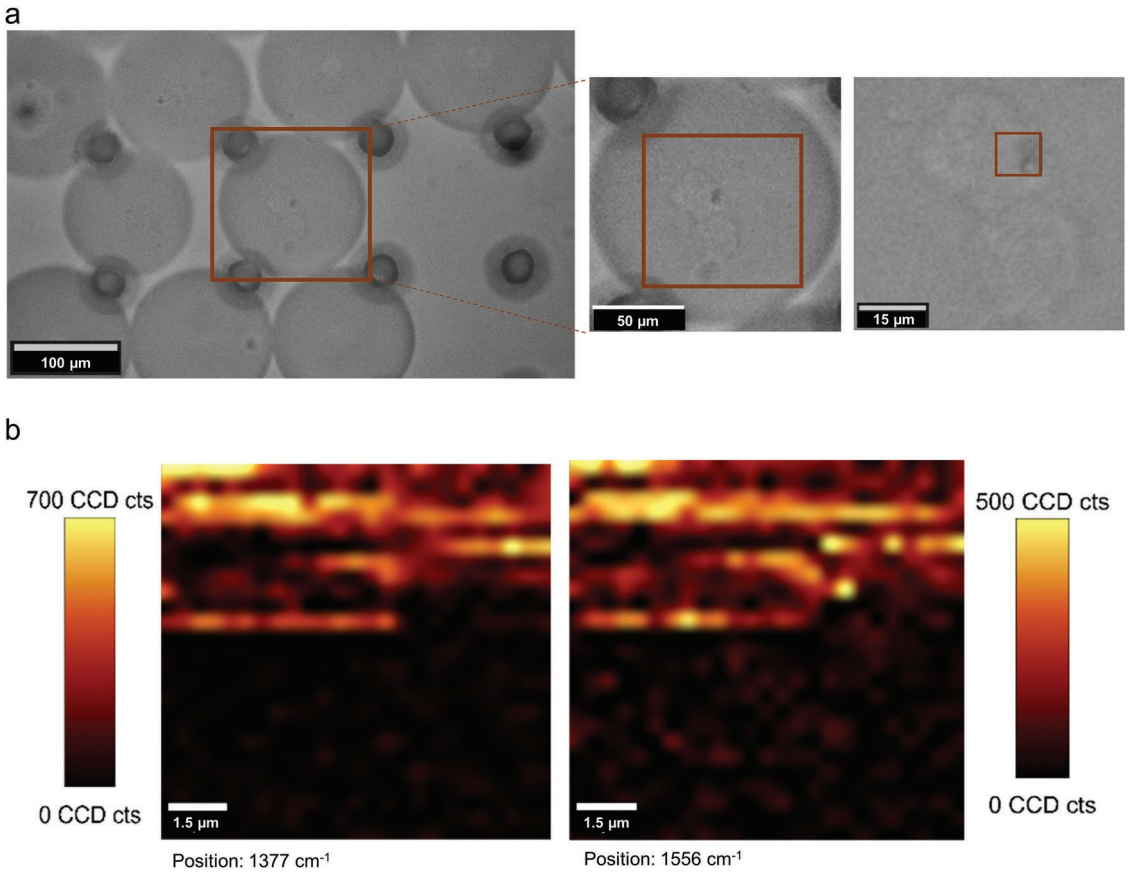

Figure 5. SERS mapping in SK-BR-3 cells, for selected peaks of 1-NAT. a) Bright-field images (20× magnification) of SK-BR-3 cells labeled with SERS tags. b) SERS intensity maps (area of 10 µm × 10 µm, 1 s and 0.8 µm step size) of the 1-NAT vibrational signatures 1377 and 1556 cm^{-1}. Scale bar is 10 µm.

and not for isolated single cells.[69] Also, it has been recently published that the use of label-free SERS combined with microdroplets for the metabolic activity exploration of single cells.[70] In this work, it should be noted that for the final multiplexing experiment (Figure 7), different areas within the cell surface may provide differences in the intensity of the peaks, related to the expression of the cell membrane receptors. For this specific experiment, as expected, we observed the 1-NAT characteristic peaks, which report the presence of the EpCAM protein on the cell surface, although with low levels of expression. On the other end, both TB and NB (paired to Vimentin and CD45, respectively) do not appear on the combined acquired spectra. The latter was expected as Vimentin is not expressed in the membrane of the cells, and CD45 is only expressed in hematopoietic cells. Those two biomarkers were used as negative controls to study possible non-specific interactions of the codified NPs with the cells, in the presence of antibodies. Vimentin was intentionally used, due to its intracellular expression, to verify that the SERS tags did not penetrate through the membrane of the cells. The immunofluorescence assay (Figure S7, Supporting Information) confirmed that, as expected, MDA-MB-435 cells were positive for EpCAM and Vimentin and negative for CD45. EpCAM is an intermembrane biomarker, while Vimentin is mostly expressed in the intracellular part of the cells. However, SERS tags are designed to bind at the membrane surface level, and not to be internalized by the cells.

These results show for the first time the multiplex and single-cell characterization of cancer single-cells in microdroplets. This work opens up the possibility of increasing the number of biomarkers, which could also be used with other cell lines, and for different types of cancer. In the future, once this process is tested across different cell lines, this methodology could be applied to the analysis of cells from cancer patients, having the capacity of providing not only qualitative but also quantitative data regarding the cell expression level. The latter allows the possibility of discrimination of biomarkers that are associated with a worse prognosis, higher malignancy, and colonization capacity of cells. For example, the phenotypic profile of specific cells like CTCs has demonstrated clinical relevance, and this technique could be applied to the characterization of these types of cells. This technology could be of extreme importance to be able to provide oncologists with a full profile of the phenotype of CTCs, allowing informed therapeutic decisions toward fully personalized medicine. In conclusion, this work paves the way toward the multiplex phenotyping of single cancer cells in a fast, reproducible, and quantitative way.

4. Experimental Section

Materials: All chemicals were purchased from Merck, and all products were used as received. Milli-Q ultrapure water (Millipore, Burlington, MA, USA) was used throughout all the experiments.

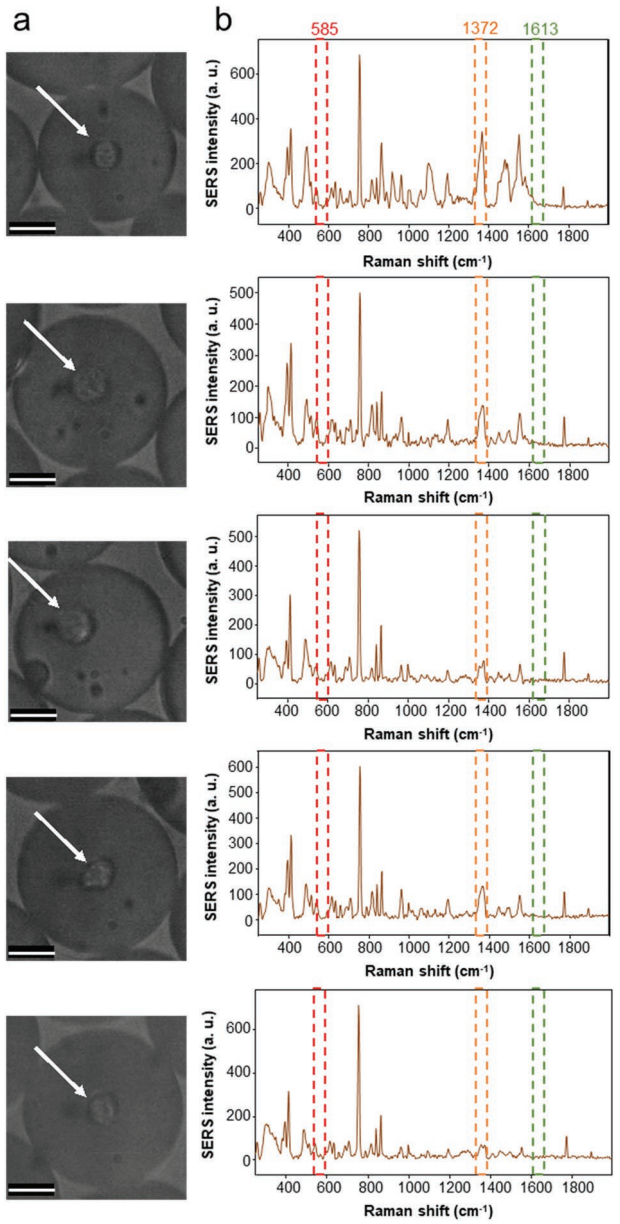

Figure 6. Spectroscopic analysis of the phenotypic profile of five MDA-MB-435 cells encapsulated in droplets and labeled with GNSs@RaR@Ab: GNSs@1-NAT@EpCAM, GNSs@TB@Vimentin, and GNSs@NB@CD45. For this experiment 6×10^4 NPs cell^{-1} were mixed with 1×10^5 MDA-MB-435 cells off-chip following encapsulation. a) Five bright-field images of five different cells containing microdroplets. b) SERS results after measurements in each cell. The selected characteristic peaks were: at 1372 cm^{-1} for 1-NAT; at 1613 cm^{-1} for TB, and 585 cm^{-1} for NB, and highlighted in dashed boxes in orange, green, and red, respectively. Scale bar 50 µm.

Synthesis of Gold Nanostars: GNSs were synthesized using a modification of a seed-mediated growth previously reported.[37] Initially, the Turkevich method[71] was used to produce 15 nm gold spherical NPs that were used as seeds. Briefly, 100 mL of a solution of chloroauric acid ($HAuCl_4$) at 0.5 mM was heated under magnetic stirring, and after boiling, 5 mL of a sodium citrate dihydrate solution (1%) was quickly added. The mixture was kept under magnetic stirring until it turned from a light yellow to a dark red color. After, polyvinylpyrrolidone (PVP)-10 K was added to the previous solution, considering that 60 molecules of PVP per nm^2 were needed for the coating of the seeds previously synthesized. The solution was left overnight under vigorous stirring. The resulting dispersion was then centrifuged at 7000 rpm for 90 min and re-dispersed in the same volume of IPA. The resulting PVP-coated gold (Au@PVP) seeds were stored in the fridge until further use. For the seed-mediated growth of the GNSs, 25 g of PVP-10K were dissolved in 250 mL of N, N-dimethylformamide (DMF) using an ultrasound sonicator, for 15 min. Then, 1 mL of 0.126 M $HAuCl_4$ was added and vigorously magnetically stirred for 2 min, to allow the Au^{3+} to be reduced to Au^{1+}. Afterward, 1.3 mL of Au@PVP seeds (1.8×10^{-3} M) was added to the reaction flask and the reaction was left under magnetic stirring for 1 h. The resulting GNSs were washed six times (4000 rpm, 30 min) with IPA to remove excess PVP and DMF and stored in IPA protected from the light until further use.

Raman Reporter Codification and Silica Coating of Gold Nanostars: To perform the codification step of the GNSs, MUA, RaRs, at final concentrations of 10 µM and 10^{-4} M respectively, and 8.5 µL of ammonium hydroxide (NH_4OH 29%) were sequentially added to aliquots of 2 mL of the GNSs previously synthesized. The RaRs used in the experiments were: 1-NAT, TB, and NB. The resulting solutions were left under magnetic stirring for 2 h, followed by a washing step at 2500 rpm for 30 min, and redispersed in 2 mL of IPA.

After the codification process, the GNSs were coated with a thin silica layer, using a modification of the Stöber method.[72] Briefly, 9.72 µL of tetraethyl orthosilicate (TEOS), 100 µL of Mili-Q water, and 8.4 µL of NH_4OH 29% were added to the solutions of codified GNSs. The mixture was placed in the orbital shaker overnight, followed by three washing steps, centrifugations at 3000 rpm for 30 min, and redispersed in 2 mL of IPA. The GNSs@RaR@SiO_2 were then stored until further use in IPA and protected from the light.

Bioconjugation with Antibodies: For the GNS, the three different batches of GNSs@RaR@SiO_2, with a concentration of 1 mM of gold, were centrifuged at 4000 rpm for 10 min and re-dispersed in PBS (1 mM, pH 7.4) with 0.05% of Tween-20 (PBS-T). Next, to the batches of GNSs@RaR@SiO_2 (1 mL each), carboxyethyl silanetriol (CTS) was added, taking into account the surface area (1 molecule of CTS per nm^2). The resulting dispersion was placed under magnetic stirring for 3 h, centrifuged at 4000 rpm for 15 min, and re-dispersed in the same volume (1 mL) of PBS-T. For the activation of the carboxylic group of the CTS, 100 µL of a buffer solution of 2% EDC / 3% NHS was added, respectively, to each batch of GNSs. Then, the dispersions were put in the orbital shaker, for 15 min for GNS@RaR@SiO_2, centrifuged (2500 rpm, 5 min), and re-dispersed in PBS-T. Then, for the antibody conjugation with the NPs, an antibody for the EpCAM was paired to each individual solution of the GNSs@1-NAT@SiO_2@CTS to a final concentration of antibody of 0.01 mg mL^{-1}.

Finally, for the multiplexing assay, GNSs were also conjugated with an antibody for Vimentin, which was paired to the GNSs@TB and an antibody for the leukocyte common antigen (CD45) was paired to the GNSs@NB. All solutions were placed in the orbital shaker for 2 h, then centrifuged three times at 2000 rpm for 2 min, and re-dispersed in PBS (1 mM, pH 7.4). After the final washing step, they were re-dispersed in PBS (0.1 mM, pH 7.4).

Cell Labeling with SERS Tags: For the first labeling of codified NPs with cancer cells, the SK-BR-3 cell line was used. For that, a total of 3×10^4 codified GNSs per each SK-BR-3 cell were used, in 100 µL of PBS-T (0.05%) for GNSs. In addition, control samples based on SK-BR-3 cells labeled with codified GNSs without antibodies were used. Besides that, four solutions of SK-BR-3 cells were prepared, each solution containing 1×10^5 cells in 100 µL of PBS (1 mM).

The same process was performed for the three batches of codified GNSs that were labeled with MDA-MB-435, only the number of NPs per cell was modified, using 6×10^4 NPs per cell.

The resulting mixture of cells and codified NPs was put into the orbital shaker (30 rpm at room temperature) for 2 h, and then the solutions were centrifuged (3× at 2500 rpm, 2 min) and re-dispersed in PBS (0.1 mM).

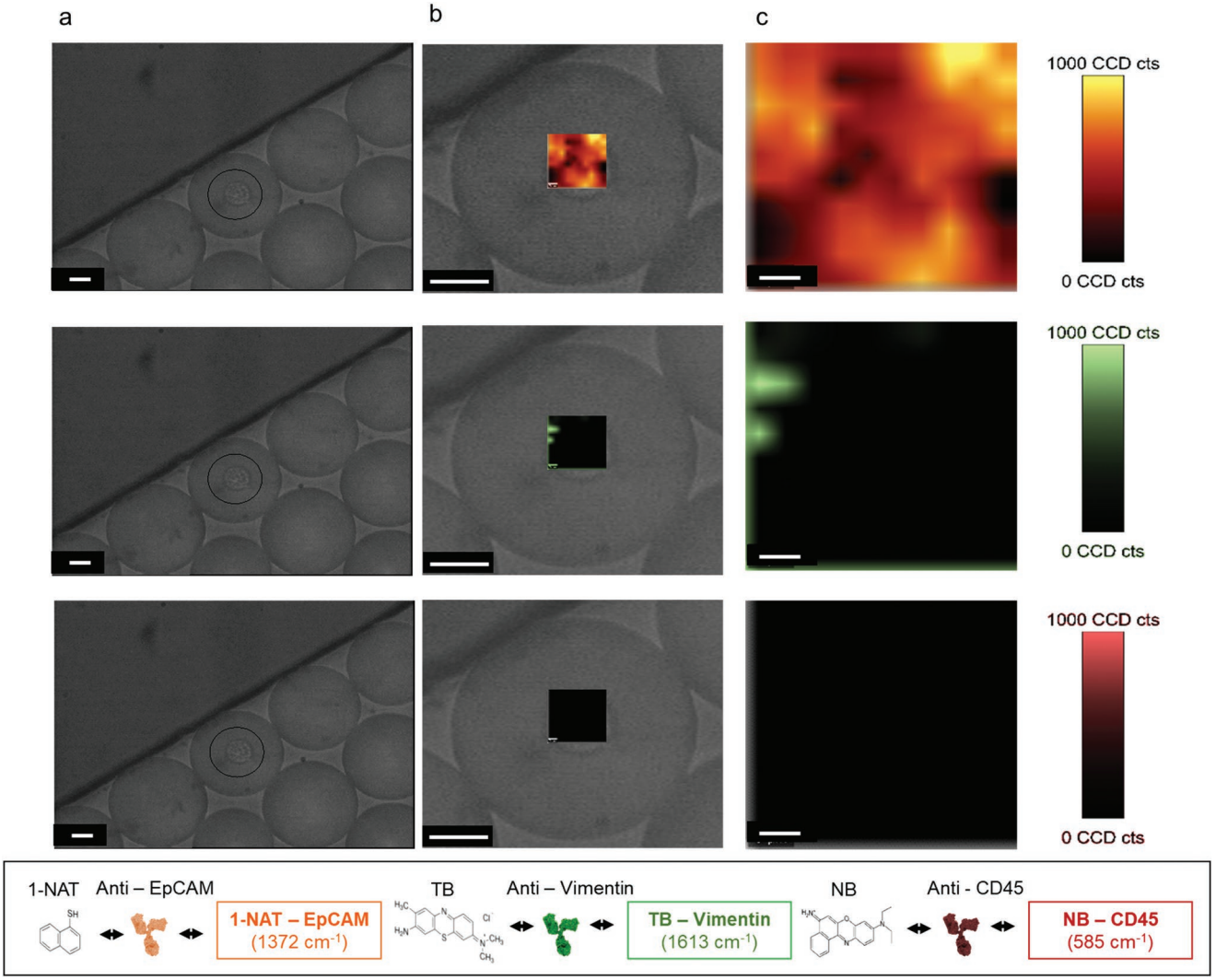

Figure 7. Multiplex phenotypic characterization of MDA-MB-435 cells using three different SERS tags. a) Bright-field images (objective 10×; scale bar 20 µm) of an MDA-MB-435S cell labeled with GNSs@RaR encapsulated in a microdroplet. b) High magnification image (objective 20×; scale bar 20 µm) and overlay of SERS mapping on top of a single cell. c) Respective SERS intensity maps (area of 20 µm × 20 µm, 1 µm step size) for each RaR, and corresponding intensity color scale (scale bar 3 µm). Inset: Pairing of RaRs with specific antibodies for recognition of cell membrane receptors. EpCAM was paired to 1-NAT and was expected a SERS signal due to the expression of EpCAM in the surface of MDA-MB-435 cells; Vimentin was paired to TB and no signal was expected as this is an intracellular protein; CD45 was included as a negative control as it is not expressed in the cancer cell line used for this study.

Microfluidic Device Design and Fabrication: A photolithographic process was followed for the fabrication of SU-8 2025 (photoresist, MicroChem) molds that were subsequently used for PDMS devices replica fabrication. All processes regarding the fabrication of the SU-8 molds were executed within a class 100 (according to the FED STD 209E, in ISO 14644-1 standard is the ISO 5) micro and nanofabrication cleanroom of around 700 m^2 effective space. The software Autodesk AutoCAD 2019 was utilized to draw the design outlines to be replicated on the master, with the completed drawings exhibited in Figures S3 and S4, Supporting Information. The AutoCAD file was processed for the direct writing laser (DWL) machine (DWL 200, Heidelberg Instruments). The pattern of the complete design was inscribed on a quartz hard mask that would confine the passage of UV light during the exposure step of the photolithography process. Approximately 5 mL of SU-8 was poured on the center of an "8" (20.32 cm) silicon wafer by spin-coating. The protocol followed for the spin-coating was a 2-step process, starting with 500 rpm for 5 s, followed by 1000 rpm for 33 s, in order to obtain an estimated layer thickness of 75 µm for the microdroplet generator. For the reservoirs used for the Raman imaging, the desired height of the resist was 120 µm. For this, the spin coating conditions described above were applied, followed by the second cycle of spin coating at 500 rpm for 5 s and 1450 rpm for 40 s. A post-bake was applied to the silicon wafers for 3 min at 65 °C followed by 9 min at 95 °C for both intended depths. The wafers were then exposed to UV light through the hard masks on a mask aligner for 10 s (lamp intensity 50 mW cm^{-2}; MA6BA6, Suss Microtech). After post-baking (1 min at 65 °C and 4 min at 95 °C) and development in SU-8 developer (PGMEA, Sigma Aldrich), the master was hard-baked for 2 min at 170 °C. For the fabrication of the PDMS (Sylgard 184) replicas, a mixture of PDMS and cross-linker (ratio 10:1, w/w) was poured on top of the master and top of an empty petri-dish, degassed, and then cured for 1 h at 65 °C. The cured device was cut and peeled off from the master, and holes for tubing were made with a biopsy punch (diameter = 1 mm; Kai Medical). The cured PDMS blank part on the empty petri-dish was peeled-off and used as a base for bonding for obtaining the final PDMS/PDMS devices.

Cell Encapsulation in Microdroplets: The encapsulation of the labeled cells with NPs was made with microdroplet generators having the design indicated in Figure S3, Supporting Information. First, two polytetrafluoroethylene (PTFE) tubing pieces (0.38 mm i.d.) were cut and inserted at the end of two syringes (Terumo, 1 mL), making sure they were long enough to reach the microfluidic device on top of the microscope (Nikon MA-200). One syringe was filled with the labeled cells solution and the other with a mixture of a fluorinated oil and surfactant (HFE 7500 (Novec) + Pico-Surf 1 (2%) (Sphere Fluidics, Ltd.)). Both syringes were mounted on two syringe pumps (New Era Pump Systems), and the tubing ends were connected to the microfluidic device. The syringe pumps were programmed to produce a flow rate ratio (Q_{oil}/Q_{cells}) of 10 between the flow rate of the oil (Q_{oil}) and the cells solution (Q_{cells}), respectively. An additional tubing piece was used to recover the droplets from the outlet of the device to run the droplets into a reservoir, once the encapsulation was stable, verifying after an inspection under the microscope. When the droplets started to fill the reservoir, a plug was inserted into the outlet of the device, and the inlet tube was burnt to make proper sealing and close the reservoir. The reservoir was used as a support for the cell containing droplets for later analysis.

SERS Characterization: Raman measurements were carried out in a 300R Confocal Raman microscope (WITec) using a 785 nm laser line grating (600 gr cm^{-1}) as the excitation source and 10× and 20× objectives. Acquisition of liquid samples, normalized to obtain a final concentration of Au of 1 mM, were performed for 1 s and five different scans (using objective 10×). The Raman power was set at 70 mW.

The different single spectra and maps from the reservoirs containing microdroplets were also acquired. Every single spectrum was performed for 1 s and five different scans and an individual spectrum of the map was acquired for 1 s with a step size of 0.8 µm using the 20× objective. For the multiplexing analysis, the map was acquired for 1 s with a step size of 1 µm using the 20× objective. The Raman power was set at 70 mW. SERS spectra were processed with the Project4 WITec software for background and cosmic ray removal corrections and GRAMS/AI Spectroscopy software for figure preparation.

Cell Culture and Immunofluorescence Assay: SK-BR-3 (from ATCC, HTB-30) and MDA-MB-435 (from ATCC, HTB-129), two different human cancer cell lines, breast and melanoma, respectively were cultured in Dulbecco's modified Eagle's medium (DMEM; Gibco) supplemented with 10% fetal bovine serum (FBS; Gibco) and 1% Penicillin/Streptomycin (Corning) and incubated at 37 °C under 5% CO_2.

For the immunofluorescence assay, cells were seeded on sterile glass coverslips (13 mm diameter), previously treated with Poly-Lysine, placed in a 24-well plate at a density of 1×10^5 cells per well, and grown for 24 h. Afterward, cells were fixed with 2% paraformaldehyde (PFA for 30 min, permeabilized with 0.1% Triton X-100 in 0.1% sodium citrate for 10 min, and blocked with 5% BSA in PBS 0.05% Tween-20 for 30 min). In between all the previous steps, the cells were washed with PBS (10 mM, pH 7.4). For immunofluorescence staining, MDA-MB-435 cells were incubated with antibodies: anti-EpCAM Alexa Fluor 488 (Biolegend; 0.01 mg mL^{-1} in 2% BSA-PBS), anti-Vimentin eFluor 570 (eBiosciences; 0.004 mg mL^{-1} in 2% BSA-PBS) and anti-CD45 Cy5 (Immunostep; 0.02 mg mL^{-1} in 2% BSA-PBS) for 1 h, at room temperature. Cells were also stained with 0.02 mg mL^{-1} of 4′, 6-diamidino-2-phenylindole (DAPI) that binds regions in DNA, staining the cell nuclei. A fluorescence-inverted Nikon-TI-E microscope was used for the immunostaining visualization. Images were analyzed with NIS Software.

Optical Characterization of the NPs by UV–Vis Spectroscopy: The resulting GNSs were characterized by UV–vis spectrophotometry (SHIMADZU UV-2550). UV–vis absorption spectra were acquired using a cuvette (1 cm path length). Spectral analyses were performed in the range of 300–900 nm for GNSs at room temperature.

Morphological Characterization of the NPs by Transmission Electron Microscopy: NPs were morphologically characterized using TEM (JEOL-2100). Ten microliters of the prepared colloidal GNSs samples were drop-cast onto a piece of ultrathin Formvar-coated 400-mesh copper grid (Ted Pella, INC.) and left to dry. TEM images were acquired at 200 kV and Image J was used to measure the size distribution measurements. For each sample, the size of at least 150 particles was measured and the average size and standard deviation were obtained.

Supporting Information

Supporting Information is available from the Wiley Online Library or from the author.

Acknowledgements

This work was supported by EU Framework Programme for Research and Innovation H2020 COFUND (713640 S.A.-C.); by FCT and the European Regional Development Fund (ERDF) through COMPETE2020 through the Impact-L project (030782 A.T., S.A.-C, and L.D.) and by the European Union through the call H2020-FETOPEN-2018-2020 in the framework of the BIOCELLPHE project (965018 S.A.-C. and L.D.). L.W. acknowledges funding to the CANCER project (NORTE-01-0145-FEDER-000029) co-funded through the NORTE-45-2015-02 program. A.T. acknowledges the FCT studentship SFRH/BD/148091/2019. The authors kindly thank Miguel Spuch-Calvar from MSpuchDesign for the 3D illustrations.

Conflict of Interest

The authors declare no conflict of interest.

Author Contributions

K.O. and A.T. contributed equally to this work. S.A.-C. and L.D. contributed to conceptualization and ideation: S.A.-C., K.O., A.T., J.M.F. and L-R.-L. contributed to the experimental execution of the work and data interpretation; C.L., P.P., and L.W. contributed to cell culture and immunofluorescence assays; S.A.C., A.T., and K.O. contributed to the original draft preparation, and all authors contributed to the final revision of the manuscript before submission. All authors have read and agreed to the final version of the manuscript.

Data Availability Statement

The data that support the findings of this study are available from the corresponding author upon reasonable request.

Keywords

cancer, microdroplets, multiplexing, single cells, surface-enhanced Raman scattering

Received: June 28, 2022
Revised: September 16, 2022
Published online: November 14, 2022

[1] World Health Organization – Cancer, https://www.who.int/health-topics/cancer
[2] A. S. B. Primeau, Cancer Recurrence Statistics, **2018**, https://www.cancertherapyadvisor.com/home/tools/fact-sheets/cancer-recurrence-statistics/.

[3] D. R. Welch, D. R. Hurst, *Cancer Res.* **2019**, *79*, 3011.
[4] C. L. Chaffer, R. A. Weinberg, *Science* **2011**, *331*, 1559.
[5] P. Bheda, R. Schneider, *Trends Cell Biol.* **2014**, *24*, 712.
[6] G. Zhan, W. Wang, H. Sun, Y. Hou, L. Feng, *Cyborg Bionic. Syst.* **2022**, *2022*, 9842349.
[7] K. Kant, S. Abalde-Cela, *Biosensors* **2018**, *8*, 62.
[8] S. Mashaghi, A. Abbaspourrad, D. A. Weitz, A. M. van Oijen, *TrAc, Trends Anal. Chem.* **2016**, *82*, 118.
[9] G. M. Whitesides, *Nature* **2006**, *442*, 368.
[10] N. W. Choi, M. Cabodi, B. Held, J. P. Gleghorn, L. J. Bonassar, A. D. Stroock, *Nat. Mater.* **2007**, *6*, 908.
[11] N. K. Inamdar, J. T. Borenstein, *Curr. Opin. Biotechnol.* **2011**, *22*, 681.
[12] C. D. Chin, T. Laksanasopin, Y. K. Cheung, D. Steinmiller, V. Linder, H. Parsa, J. Wang, H. Moore, R. Rouse, G. Umviligihozo, E. Karita, L. Mwambarangwe, S. L. Braunstein, J. van de Wijgert, R. Sahabo, J. E. Justman, W. El-Sadr, S. K. Sia, *Nat. Med.* **2011**, *17*, 1015.
[13] S.-Y. Teh, R. Lin, L.-H. Hung, A. P. Lee, *Lab Chip* **2008**, *8*, 198.
[14] P. Gravesen, J. Branebjerg, O. S. Jensen, *J. Micromech. Microeng.* **1993**, *3*, 168.
[15] H. A. Stone, A. D. Stroock, A. Ajdari, *Annu. Rev. Fluid Mech.* **2003**, *36*, 381.
[16] G. M. Whitesides, A. D. Stroock, *Phys. Today* **2001**, *54*, 42.
[17] P. Li, X. Liu, M. Kojima, Q. Huang, T. Arai, *Langmuir* **2021**, *37*, 8083.
[18] A. B. Theberge, F. Courtois, Y. Schaerli, M. Fischlechner, C. Abell, F. Hollfelder, W. T. S. Huck, *Angew. Chem., Int. Ed.* **2010**, *49*, 5846.
[19] L. Mazutis, J. Gilbert, W. L. Ung, D. A. Weitz, A. D. Griffiths, J. A. Heyman, *Nat. Protoc.* **2013**, *8*, 870.
[20] C. N. Baroud, F. Gallaire, R. Dangla, *Lab Chip* **2010**, *10*, 2032.
[21] Q. Zhang, T. Wang, Q. Zhou, P. Zhang, Y. Gong, H. Gou, J. Xu, B. Ma, *Sci. Rep.* **2017**, *7*, 41192.
[22] S. Hasan, D. Geissler, K. Wink, A. Hagen, J. J. Heiland, D. Belder, *Lab Chip* **2019**, *19*, 403.
[23] R. Best, S. Abalde-Cela, C. Abell, A. G. Smith, *Curr. Biotechnol.* **2016**, *5*, 109.
[24] A. F. Vallejo, J. Davies, A. Grover, C.-H. Tsai, R. Jepras, M. E. Polak, J. West, *iScience* **2021**, *24*, 102147.
[25] K. Matuła, F. Rivello, W. T. S. Huck, *Adv. Biosyst.* **2020**, *4*, 1900188.
[26] J. L. Paris, F. Coelho, A. Teixeira, L. Diéguez, B. F. B. Silva, S. Abalde-Cela, *Molecules* **2020**, *25*, 3277.
[27] Y. Zhu, Q. Fang, *Anal. Chim. Acta* **2013**, *787*, 24.
[28] Y. Yin, T. Qiu, W. Zhang, P. K. Chu, *J. Mater. Res.* **2011**, *26*, 170.
[29] S. Schlücker, *Angew. Chem., Int. Ed.* **2014**, *53*, 4756.
[30] R. A. Alvarez-Puebla, L. M. Liz-Marzán, *Small* **2010**, *6*, 604.
[31] L. Rodríguez-Lorenzo, M. Spuch-Calvar, S. Abalde-Cela, in *SERS for Point-of-care and Clinical Applications* (Ed: A. Fales), Elsevier, Amsterdam, Oxford, Cambridge **2022**, pp. 53–88.
[32] J. Lee, D. Y. Hyeon, D. Hwang, *Exp. Mol. Med.* **2020**, *52*, 1428.
[33] M. Constantinou, K. Hadjigeorgiou, S. Abalde-Cela, C. Andreou, *ACS Appl. Nano Mater.* **2022**, *5*, 12276.
[34] A. Teixeira, J. L. Paris, F. Roumani, L. Diéguez, M. Prado, B. Espiña, S. Abalde-Cela, A. Garrido-Maestu, L. Rodriguez-Lorenzo, *Materials* **2020**, *13*, 1934.
[35] L. Fabris, *ChemNanoMat* **2016**, *2*, 249.
[36] L. Rodríguez-Lorenzo, A. Garrido-Maestu, A. K. Bhunia, B. Espiña, M. Prado, L. Diéguez, S. Abalde-Cela, *ACS Appl. Nano Mater.* **2019**, *2*, 6081.
[37] P. S. Kumar, I. Pastoriza-Santos, B. Rodríguez-González, F. J. G. de Abajo, L. M. Liz-Marzán, *Nanotechnology* **2008**, *19*, 015606.
[38] B. Mir-Simon, I. Reche-Perez, L. Guerrini, N. Pazos-Perez, R. A. Alvarez-Puebla, *Chem. Mater.* **2015**, *27*, 950.
[39] N. Pazos-Perez, J. M. Fitzgerald, V. Giannini, L. Guerrini, R. A. Alvarez-Puebla, *Nanoscale Adv.* **2019**, *1*, 122.
[40] J. Smolsky, S. Kaur, C. Hayashi, S. Batra, A. Krasnoslobodtsev, *Biosensors* **2017**, *7*, 7.
[41] S. Barbosa, A. Agrawal, L. Rodríguez-Lorenzo, I. Pastoriza-Santos, R. A. Alvarez-Puebla, A. Kornowski, H. Weller, L. M. Liz-Marzán, *Langmuir* **2010**, *26*, 14943.
[42] R. A. Alvarez-Puebla, D. S. Dos Santos Jr, R. F. Aroca, *Analyst* **2004**, *129*, 1251.
[43] T. Hiraga, S. Ito, H. Nakamura, *Int. J. Cancer* **2016**, *138*, 1698.
[44] A. Martowicz, G. Spizzo, G. Gastl, G. Untergasser, *BMC Cancer* **2012**, *12*, 501.
[45] N. Nivedita, P. Ligrani, I. Papautsky, *Sci. Rep.* **2017**, *7*, 44072.
[46] R. Mažeikienė, G. Niaura, O. Eicher-Lorka, A. Malinauskas, *Vib. Spectrosc.* **2008**, *47*, 105.
[47] Y. Wu, Y. Jiang, X. Zheng, S. Jia, Z. Zhu, B. Ren, H. Ma, *R. Soc. Open Sci.* **2019**, *5*, 172034.
[48] D. L. Holliday, V. Speirs, *Breast Cancer Res.* **2011**, *13*, 215.
[49] K. Hoshino, G. Bhave, E. Ng, X. Zhang, *Sens. Actuators, A* **2014**, *216*, 301.
[50] A. M. Sieuwerts, J. Kraan, J. Bolt, P. van der Spoel, F. Elstrodt, M. Schutte, J. W. M. Martens, J.-W. Gratama, S. Sleijfer, J. A. Foekens, *J. Natl. Cancer Inst.* **2009**, *101*, 61.
[51] U. Schnell, V. Cirulli, B. N. G. Giepmans, *Biochim. Biophys. Acta, Biomembr.* **2013**, *1828*, 1989.
[52] A. Satelli, S. Li, *Cell. Mol. Life Sci.* **2011**, *68*, 3033.
[53] M. Kokkinos, R. Wafai, M. Wong, D. Newgreen, E. Thompson, M. Waltham, *Cells Tissues Organs* **2007**, *185*, 191.
[54] I. S. Trowbridge, M. L. Thomas, *Annu. Rev. Immunol.* **1994**, *12*, 85.
[55] G. Bodelón, V. Montes-García, J. Pérez-Juste, I. Pastoriza-Santos, *Front. Cell Infect. Microbiol.* **2018**, *8*, 143.
[56] J. Reguera, J. Langer, D. J. de Aberasturi, L. M. Liz-Marzán, *Chem. Soc. Rev.* **2017**, *46*, 3866.
[57] L. Rodriguez-Lorenzo, L. Fabris, R. A. Alvarez-Puebla, *Anal. Chim. Acta* **2012**, *745*, 10.
[58] J.-M. Li, C. Wei, W.-F. Ma, Q. An, J. Guo, J. Hu, C.-C. Wang, *J. Mater. Chem.* **2012**, *22*, 12100.
[59] M. Li, J. W. Kang, S. Sukumar, R. R. Dasari, I. Barman, *Chem. Sci.* **2015**, *6*, 3906.
[60] U. S. Dinish, G. Balasundaram, Y.-T. Chang, M. Olivo, *Sci. Rep.* **2015**, *4*, 4075.
[61] C. L. Zavaleta, B. R. Smith, I. Walton, W. Doering, G. Davis, B. Shojaei, M. J. Natan, S. S. Gambhir, *Proc. Natl. Acad. Sci. U. S.A.* **2009**, *106*, 13511.
[62] D. J. de Aberasturi, A. B. Serrano-Montes, J. Langer, M. Henriksen-Lacey, W. J. Parak, L. M. Liz-Marzán, *Chem. Mater.* **2016**, *28*, 6779.
[63] L. Rodríguez-Lorenzo, R. A. Álvarez-Puebla, I. Pastoriza-Santos, S. Mazzucco, O. Stéphan, M. Kociak, L. M. Liz-Marzán, F. J. García de Abajo, *J. Am. Chem. Soc.* **2009**, *131*, 4616.
[64] L. Rodríguez-Lorenzo, R. A. Álvarez-Puebla, F. J. G. de Abajo, L. M. Liz-Marzán, *J. Phys. Chem. C* **2010**, *114*, 7336.
[65] C. Hrelescu, T. K. Sau, A. L. Rogach, F. Jäckel, J. Feldmann, *Appl. Phys. Lett.* **2009**, *94*, 153113.
[66] J.-R. Lin, M. Fallahi-Sichani, P. K. Sorger, *Nat. Commun.* **2015**, *6*, 8390.
[67] L. Wu, A. Teixeira, A. Garrido-Maestu, L. Muinelo-Romay, L. Lima, L. L. Santos, M. Prado, L. Diéguez, *Biosens. Bioelectron.* **2020**, *165*, 112392.
[68] S. Abalde-Cela, L. Wu, A. Teixeira, K. Oliveira, L. Diéguez, *Adv. Opt. Mater.* **2021**, *9*, 2001171.
[69] Z. A. Nima, M. Mahmood, Y. Xu, T. Mustafa, F. Watanabe, D. A. Nedosekin, M. A. Juratli, T. Fahmi, E. I. Galanzha, J. P. Nolan, A. G. Basnakian, V. P. Zharov, A. S. Biris, *Sci. Rep.* **2014**, *4*, 4752.
[70] D. Sun, F. Cao, Y. Tian, A. Li, W. Xu, Q. Chen, W. Shi, S. Xu, *Anal. Chem.* **2019**, *91*, 15484.
[71] J. Turkevich, P. C. Stevenson, J. Hillier, *Discuss. Faraday Soc.* **1951**, *11*, 55.
[72] W. Stöber, A. Fink, E. Bohn, *J. Colloid Interface Sci.* **1968**, *26*, 62.